Lasers Med Sci (2010) 25:259–267
DOI 10.1007/s10103-009-0723-y

ORIGINAL ARTICLE

Apoptosis- and necrosis-induced changes in light attenuation measured by optical coherence tomography

Freek J. van der Meer · Dirk J. Faber · Maurice C. G. Aalders · Andre A. Poot · Istvan Vermes · Ton G. van Leeuwen

Received: 29 December 2008 / Accepted: 31 July 2009 / Published online: 10 September 2009

Abstract Optical coherence tomography (OCT) was used to determine optical properties of pelleted human fibroblasts in which necrosis or apoptosis had been induced. We analysed the OCT data, including both the scattering properties of the medium and the axial point spread function of the OCT system. The optical attenuation coefficient in necrotic cells decreased from 2.2 ± 0.3 mm^{-1} to 1.3 ± 0.6 mm^{-1}, whereas, in the apoptotic cells, an increase to 6.4 ± 1.7 mm^{-1} was observed. The results from cultured cells, as presented in this study, indicate the ability of OCT to detect and differentiate between viable, apoptotic, and necrotic cells, based on their attenuation coefficient. This functional supplement to high-resolution OCT imaging can be of great clinical benefit, enabling on-line monitoring of tissues, e.g. for feedback in cancer treatment.

Freek J. van der Meer and Dirk J. Faber contributed equally to the manuscript and the study

F. J. van der Meer · D. J. Faber · M. C. G. Aalders · T. G. van Leeuwen
Department of Biomedical Engineering and Physics, Academic Medical Center, University of Amsterdam, Amsterdam, The Netherlands

D. J. Faber
Ophthalmology Department, Academic Medical Center, University of Amsterdam, Amsterdam, The Netherlands

A. A. Poot · I. Vermes
Polymer Chemistry and Biomaterials Group, University of Twente, Institute of Biomedical Technology, Enschede, The Netherlands

T. G. van Leeuwen (✉)
Biophysical Engineering Group, University of Twente, Institute of Biomedical Technology, P.O. Box 217, 7500 AE Enschede, The Netherlands
e-mail: t.g.vanleeuwen@amc.uva.nl

Keywords Optical coherence tomography · Optical properties · Cells · Apoptosis · Necrosis

Introduction

In every multi-cellular organism a delicate balance exists between cell division, on one hand, and cell death, on the other hand. Cell death can be executed by two different pathways, necrosis and apoptosis [1]. Necrosis, the pathological pathway, is also known as accidental cell death, which is triggered by external disturbances, e.g. physical trauma, chemical stress or hypoxia. Its morphology is characterized by slight initial cellular swelling, followed by cell lysis. In vivo, the resulting cell debris triggers an inflammatory response.

The physiological pathway of cell death is called apoptosis, also known as programmed cell death. It is a general mechanism for the clearance of cells that have become superfluous or show an aberrant function, without causing inflammation. The apoptotic pathway is conducted by a series of tightly regulated biochemical processes in which a cell, once triggered, goes through consecutive phases of cell shrinkage, chromatin condensation and breakdown, nuclear disintegration, cell blebbing and the formation of so-called apoptotic bodies. These apoptotic bodies contain nuclear fragments and cell organelles (Fig. 1). Under normal physiological conditions they are cleared by either macrophages or neighbouring cells through phagocytosis [2].

As the physiological counterpart of cell growth, apoptosis plays an important role in the balance of tissue dynamics. Disturbances in this balance results in disease. If aberrant cells do not undergo apoptosis, a tumour can develop. On the other hand, excessive apoptosis can result in degenerative

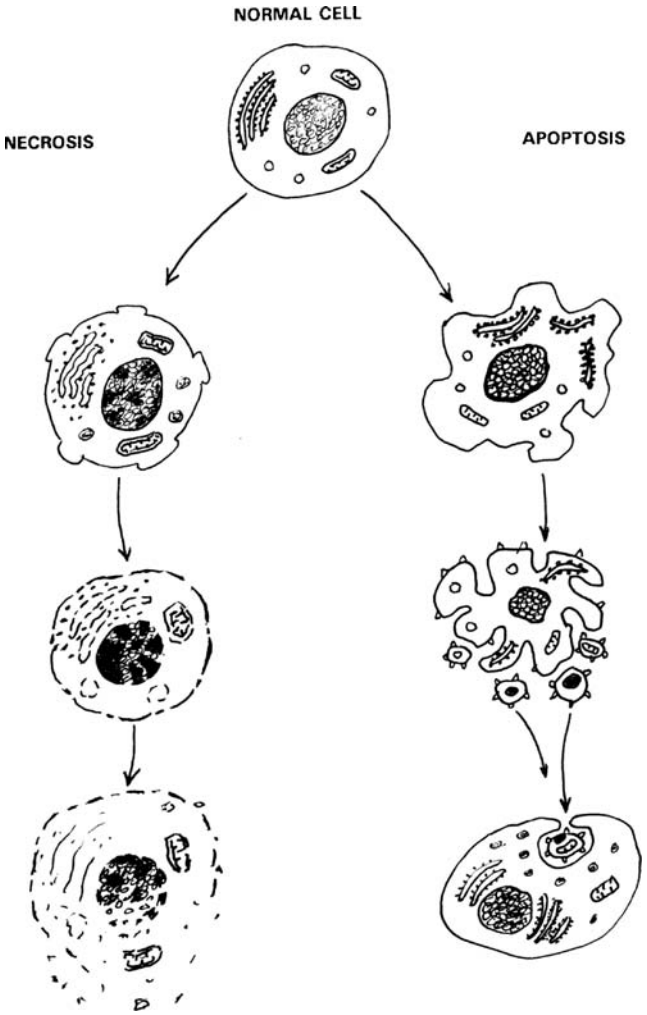

Fig. 1 Schematic representation of the different stages of necrosis (*left*) and apoptosis (*right*). The process of necrosis starts with membrane defects, followed by karyolysis and enzyme release, due to cell disintegration. Once apoptosis has been triggered in a normal cell (*top*), the membrane will change, leading to surface protrusions. The condensed nucleus fragments, which is followed by disintegration of the whole cell into apoptotic bodies, containing remnants of the nucleus and other cell components. Apoptotic bodies are cleared by phagocytosis by macrophages or neighbouring cells, or they undergo secondary necrosis

syndromes, such as atrophy and cardiomyopathy [3]. In clinical practice, treatment of these symptoms and diseases involves reduction or stimulation of apoptosis, respectively. Consequently, there is a strong need for methods that can detect and quantify apoptosis on a microscopic level. Currently, the standard methods of apoptosis detection in tissue are histological or biochemical, which are time consuming and require biopsies [4]. In vivo detection using radionuclide imaging [5] and magnetic resonance imaging [6] is currently under investigation.

Recently, Czarnota and co-workers reported that apoptosis could be detected by high-frequency ultrasound [7]. They observed an increase in backscattering of the ultrasound signal, which they attributed to the disintegration of the nucleus, a distinctive feature of apoptosis. Optical coherence tomography (OCT) imaging, the optical and high-resolution equivalent of ultrasound imaging, is based on time of flight-dependent intensity differences of backscattered light [8]. In a previous study we used OCT to image porcine carotid arteries in ex vivo tissue culture [9]. We reported an increase in backscattering in the medial layer after balloon dilation. Since there is a rapid onset of apoptosis after balloon angioplasty [10], we hypothesized that the changes in OCT signal could be attributed to this characteristic form of cell death. Functional OCT allows the quantitative measurement of tissue absorption and scattering properties, at the microscopic level. Because both apoptosis and necrosis directly influence the cell's main scatterers (i.e. nucleus, membrane, mitochondria, and other cellular organelles [11–16]), we hypothesized that the local optical attenuation coefficient (μ_t), which describes the decay of measured intensity against. depth, could be used to assess cell death. Moreover, due to the differences in the morphology of the two pathways of cell death, we hypothesized that differences could be observed in the attenuation of light by necrotic and apoptotic cells compared with that by normal cells and that those changes could be monitored in time, after induction of cell death. In this paper, we describe OCT measurements of the optical attenuation coefficient of pelleted human fibroblasts, in which necrosis or apoptosis had been induced.

Materials and methods

Cells and reagents

Human fibroblasts were maintained in Dulbecco's modified Eagle's medium (DMEM) (Gibco/BRL) supplemented with 10% fetal calf serum, streptomycin at 100 μg/ml and penicillin at 100 U/ml in a fully humidified atmosphere containing 5% carbon dioxide (CO_2) at 37°C. Prior to the experiment, subconfluent grown cells were trypsinized and collected by centrifugation at 500 *g* for 10 min. At time (t)=0, the pelleted cells were resuspended in DMEM containing 10% ethanol, to induce necrosis, or 200 μM cytosine arabinoside (AraC, Sigma), to induce apoptosis, or 0.1 mg/ml colchicine (CX, Sigma), to induce mitotic arrest. After 30 min incubation, the cells were pelleted and imaged by OCT for 6 h. In a second set of experiments the dose-dependency of apoptosis induction by AraC was studied. Culture flasks with subconfluent grown cells were incubated with 50 μM, 100 μM or 200 μM AraC for 2 h. The cells were trypsinized and collected by centrifugation at 500 *g* for 10 min. Pelleted cells were immersed in medium and imaged by OCT at 3 h, 6 h, 9 h, 12 h and 24 h after the induction of apoptosis. Between and during measurements the cells were kept at 37°C.

Verification of apoptosis

At the end of the OCT experiment, samples of pelleted cells were subjected to immunofluorescence analysis, using a commercially available apoptosis detection kit (Sigma). The double-labelling assay with annexin V-Cy3 (AnnV) and 6-carboxyfluorescein diacetate (CFDA) allows differentiation between apoptotic, necrotic and viable cells. The CFDA is processed in metabolically active cells into fluorescing 6-carboxyfluorescein (6-CF). The AnnV-Cy3 label binds to phosphatidyl serine residues when they appear in the outer leaflet of the cell membrane, which occurs in compromised cells that are apoptotic or necrotic. Therefore, cells that are labelled only with 6-CF (green) are viable cells, cells labelled only with Ann-Cy3 (red) are necrotic cells, and cells stained with both are apoptotic. The cells were labelled in accordance with the manufacturer's instructions.

Flow cytometry

To measure the necrotic and apoptotic fraction after induction of cell death, we harvested cells at different time points and washed them in ice-cold 4-(2-hydroxyethyl)-1-piperazine-ethane-sulphonic acid (HEPES) buffer [10 mM HEPES, 150 mM potassium chloride (KCl), 1 mM magnesium chloride ($MgCl_2$) and 1.3 mM calcium chloride ($CaCl_2$), pH 7.4] supplemented with 1 mg/ml glucose and 0.5% (w/v) bovine serum albumin (BSA). The cells were then incubated with fluorescein isothiocyanate (FITC)-labelled annexin V (diluted 1:200 in HEPES buffer) for 15 min and washed again in HEPES buffer. Just before analysis of the samples by flow cytometry (FACSCalibur, Becton Dickinson, San Jose, CA, USA), propidium iodide (PI) was added (final concentration 5 μg/ml) to distinguish necrotic cells (annexin V−/PI+) from early apoptotic cells (annexin V+/PI−) and late apoptotic cells (annexin V+/PI+) [4]. The samples were analysed with a FACSCalibur (Becton Dickinson) instrument equipped with CellQuest software. The cytometer was calibrated by eye with the fluorochrome beads supplied by the manufacturer.

OCT imaging

The cells were imaged with a high-resolution time-domain OCT setup in which a titanium (Ti):sapphire laser (FemtoSource, Vienna, Austria), operating at a central wavelength of 800 nm with a bandwidth of 125 nm, was used as the light source. Depth scanning, by changing the length of the (optical) path in the reference arm, was performed using a so-called rapid-scanning optical delay (RSOD) line [17] in which a linear galvanometer was used. This allowed precise and constant (speed and intensity) depth ranging at the expense of reduced imaging speed. Moreover, it allowed hardware-based compensation for the dispersion mismatch between the reference arm and sample arm. In-depth scanning was performed at 25 lines per second. For this system, we measured a dynamic range of 110 dB and a free space axial resolution of 5 μm. For each cell pellet and each time point three to five b-scans were made.

Data analysis

In each b-scan, the attenuation coefficient (μ_t) of the pelleted cells was obtained in a procedure described previously [18]. In short, the depth dependence of the amplitude of the OCT signal can be described as the product of the axial point spread function (PSF) of the optics used and the attenuation of the light by the tissue structures [19–21]. An average signal of 50–100 adjacent A-scans as a function of depth was fitted to the model with μ_t as a fitting parameter, incorporating both the known location of the focus in the tissue and the previously measured depth of focus of the imaging optics.

Results

In the experiments described in this study the cells were pelleted and were proven to be viable (data not shown), as in other studies [22–24]. Qualitatively, when compared with untreated cells (Fig. 2a), the cells treated with 200 μM AraC exhibited a temporary increase in OCT signal and a decrease in imaging depth (Fig. 2b). In contrast, cells treated with 10% ethanol showed an increase in imaging depth (Fig. 2c). These observations are quantified by the measurement of μ_t of the samples in time as presented in Fig. 3. The AraC-treated cells show an initial increase in μ_t, followed by a decrease, ending up below the level of the control cells. Treatment with 10% ethanol (EtOH) results in an immediate decrease in backscatter, compared to untreated control cells.

As shown in the fluorescence images (Fig. 4), apoptosis was induced in the AraC-treated cells. Panels 4a and 4b show untreated control cells, and panels 4c and 4d show AraC-treated cells. The green fluorescence (Fig. 4a, c) is a marker for metabolically active cells (i.e. either viable or apoptotic cells), whereas the red fluorescence marks the compromised cells (i.e. necrotic or apoptotic cells). Therefore, the double-labelled cells can be discerned between viable (green), apoptotic (green and red), and necrotic (red) cells.

Since the necrotic process rapidly results in the clearance of cells by rupture of the cell membranes, the EtOH- treated cells were not visualized by fluorescence microscopy. Fluorescence-activated cell sorter (FACS) analysis can detect necrotic cells based on the scattering of remnants. The result of the cell counting is presented in Fig. 5. The decrease in average attenuation (dotted line) coincides with

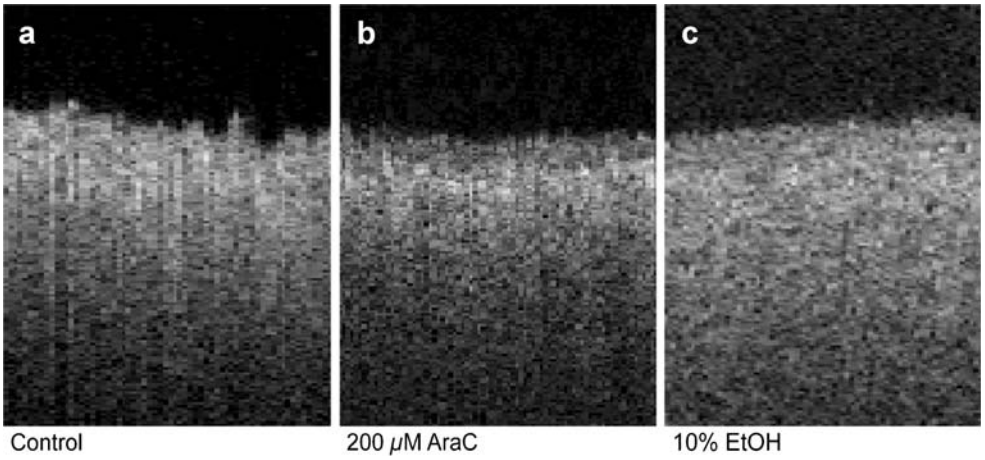

Fig. 2 Examples of OCT images of pelleted cells. Untreated control cells (**a**) remained unchanged during the entire experiment. Apoptotic AraC-treated cells (**b**) showed an increase in scattering in the top layer, whereas necrosis (**c**) resulted in a decrease in signal

a decrease in viable cells (grey line) and a synchronous increase in necrotic cells. No apoptotic cells were detected; therefore, the decreasing total cell count has to be attributed to the total clearance of necrotic cells.

The induction of apoptosis by AraC is known to be dependent on the concentration. In Fig. 6 the results are plotted of the attenuation measurement of cells treated with 50 μM (Fig. 6a), 100 μM (Fig. 6b), and 200 μM (Fig. 6c). The higher the concentration of AraC, the earlier the rise in attenuation is observed.

To study the effect of nuclear condensation on the attenuation, we treated cells with colchicine (Fig. 7). The resulting increase in μ_t mimicked the apoptosis curves.

Discussion

In the experiments described in this paper, an increase in μ_t was observed in pelleted cells after treatment with AraC. AraC is known to induce apoptosis via incorporation into DNA during replication, acting as a chain terminator [25].

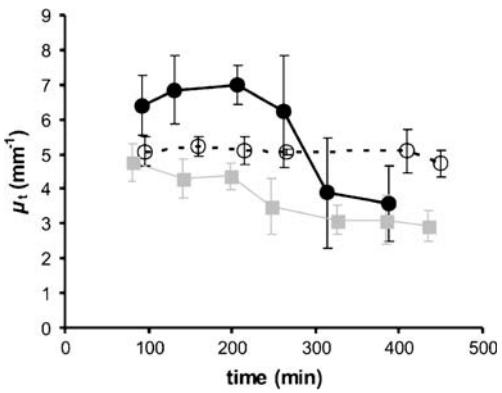

Fig. 3 The attenuation coefficient measured in pelleted human fibroblasts, as a function of time. Time was measured in minutes from the point that the cells were forced into necrosis (*filled squares*) or apoptosis (*filled dots*). Sham-treated (control) cells show no change in scattering (*circles*)

However, AraC can also induce apoptosis directly through oxidative stress, with an increase in the generation of reactive oxygen species and tumour suppressor protein 53 (p53)-dependent cytotoxicity [26, 27]. This latter, rapid, pathway has been shown to induce apoptosis in lymphoid cells within 3 hours [26]. Apart from its use in leukemia treatment, its use is known to induce apoptosis in neuronal cells [28] and fibroblasts [29].

Apoptosis was, indeed, detected with a commercially available viability assay, combining 6-CDFA with an annexin V-Cy3 label. Annexin V binds to the phosphatidyl serine that is redistributed from the inner to the outer leaflet of the plasma membrane as an early event in the apoptotic programme [30]. Binding of annexin V to externalized phosphatidyl serine has formed the basis for widely used optical methods (fluorescence microscopy and flow cytometry) for detecting apoptosis [4]. Furthermore, AraC is known to induce apoptosis in a dose-dependent fashion [31, 32]. A similar dependency was observed in the changes in μ_t in our experiments.

There is a great variety in apoptosis inducers [33]. In an experimental setup similar to the one described here, we induced apoptosis in mouse fibroblasts (MFs) with staurosporine [33], and subjected human lung carcinoma cell line (SW 1573) to 5-aminolaevulinic acid-photodynamic therapy (ALA-PDT) [34]. The preliminary results indicated that, in both cell lines, an increase in μ_t was observed (data not shown).

The origin of light scattering from cells is still the subject of studies. Scattering occurs due to the mismatch in indices of refraction between these different cellular compartments and is also dependent on the size and shape of the scatterer [11, 13, 35–37]. In the case of necrosis, the cell and its organelles disintegrate, resulting in an amorphous mass. The decrease in scattering from necrotic cells can, therefore, probably be explained by the removal of potential scatterers. On the other hand, cellular swelling prior to cell lysis might lead to an initial increase in

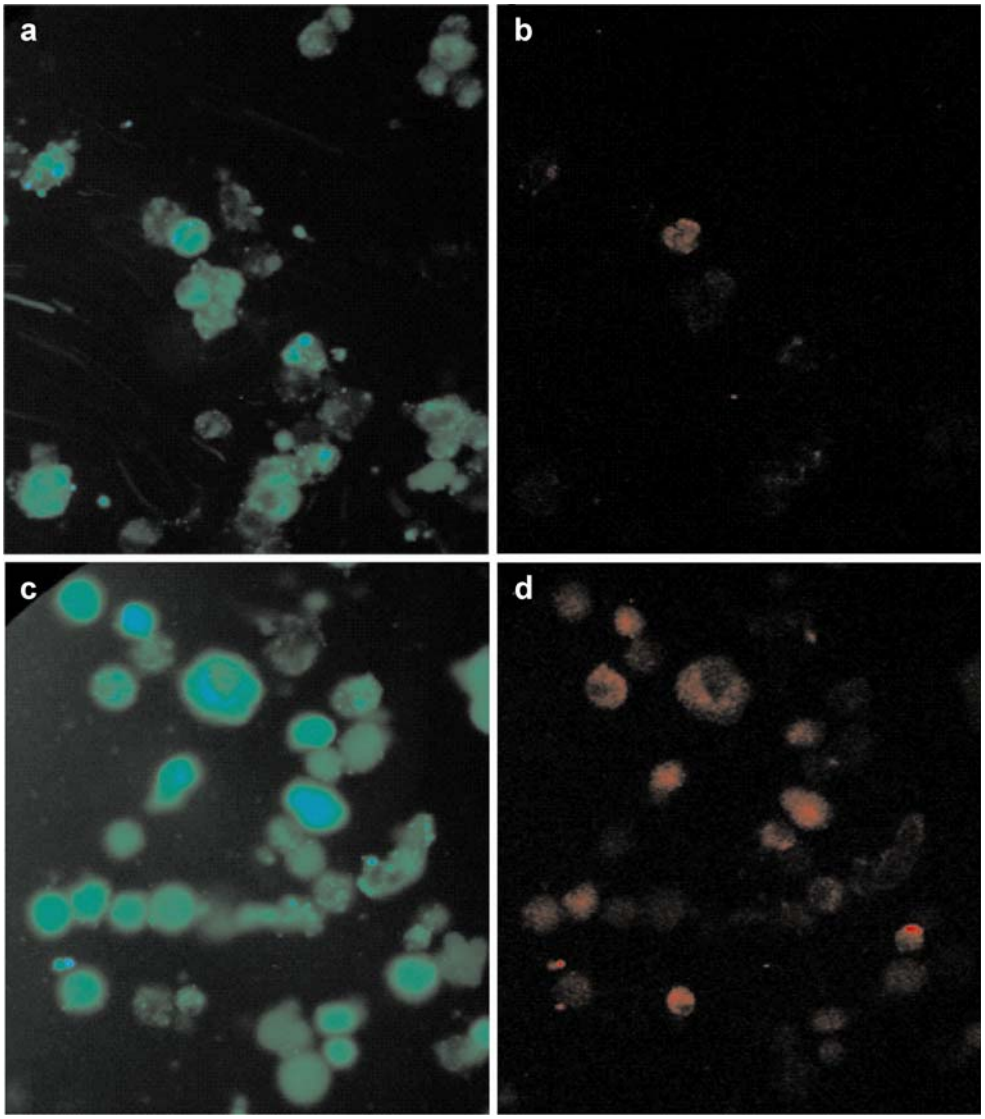

Fig. 4 Images of immunofluorescence labelling of control cells (**a**, **b**) and cells treated with 200 mM AraC (**c**, **d**) at 24 h. When the green fluorescing label CFDA (**a**, **c**) is used, viable cells can be identified, whereas the red fluorescing label AnnV (**b**, **d**) is specific for apoptotic cells. At 24 h, 5% of the control cells have become apoptotic, while, after treatment with 200 mM AraC, 61% of cells are apoptotic

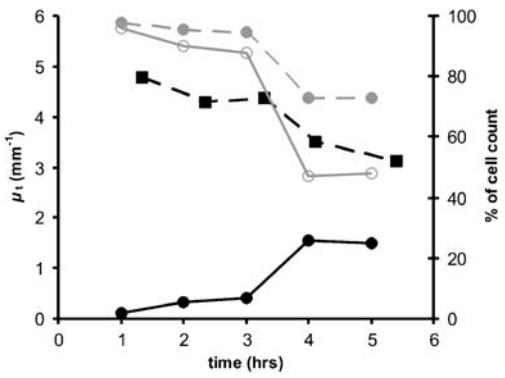

Fig. 5 After induction with 10% ethanol (t=0), the number of viable cells (*grey line, open dots*) decreases and the number of necrotic cells (*black line, filled dots*) increases. The total number of cells (*grey dotted line*) decreases, due to loss of necrotic cells. The decrease in μ_t (*black dotted line*) coincides with the increase in necrosis

scattering, which was not observed in our experiments. Valenzeno and Trank proposed a technique for measurement of the blood haematocrit based on the decrease of forward scattering during erythrocyte lysis. The loss of refractive index mismatches reduced the scattering coefficient and anisotropy [38]. The degree of haemolysis is inversely related to the intensity of small angle scattering. Furthermore, in experiments monitoring the optical density (OD) of cell suspensions, Kravtsov and Fabian reported a clear decrease in OD after the induction of necrosis [12].

The apoptotic process involves a series of morphological changes in which many potential scatterers are involved. It has been reported that the initial increase in scattering could be due to cellular shrinkage [14], to chromatin condensation [16], to nuclear fragmentation [13] or to mitochondrial swelling [39] and release of cytochrome c [40]. In investigations of mitochondrial morphology in apoptosis, single-angle light-scattering data [41] and absorption

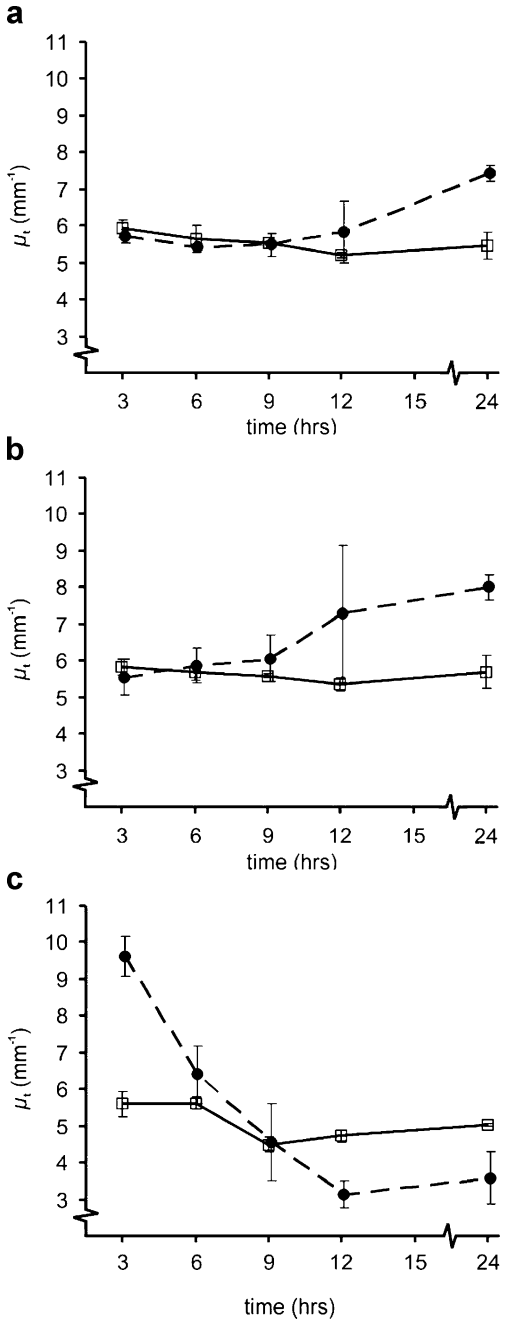

Fig. 6 Dose-dependency curves of the increase in μ_t after treatment with 50 μM (**a**), 100 μM (**b**), and 200 μM (**c**) AraC. The higher the dose, the earlier is the onset of the μ_t increase. The *black lines* depict the untreated control cells, and the *dotted lines* are AraC-treated apoptotic cells

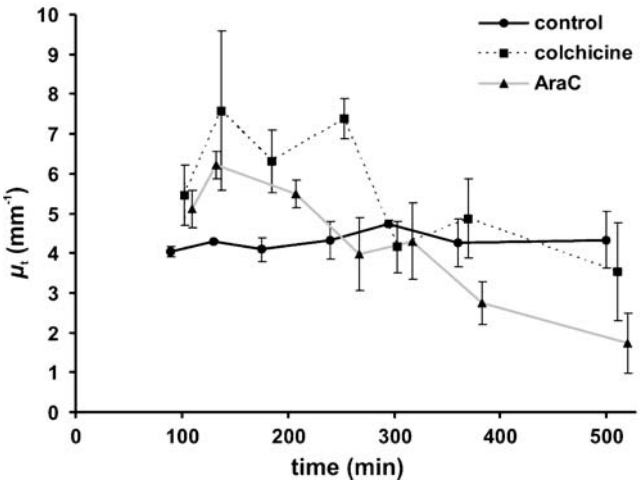

Fig. 7 Colchicine-treated cells (*black dotted line*) mimic the μ_t curve of the AraC-treated cells (*grey line*). However, the maximum values of μ_t are higher, and secondary necrosis is not significantly detected. Untreated control cells are represented by the *black line*

spectrophotometry [42] have been used to detect volume changes in suspensions of viable mitochondria isolated from apoptotic cells. Different results were obtained with these techniques (see, e.g., Kroemer et al. [43]), with some studies showing light scattering suggestive of mitochondrial swelling [41], whereas others showed no change [42]. By measuring the intensity ratio of wide-to-narrow angle scatter in single cells during apoptosis researchers have shown that the changes in the mitochondrial membrane preceded the exposure to phosphatidyl serine [44].

Kravtsov and co-workers [12] designed an assay in which they monitored the OD of cells in suspension. When inducing apoptosis, they observed a temporary increase in OD, comparable to the increase in μ_t in this study. Morphological analysis of their samples revealed that the increase in OD coincided with the blebbing of the apoptotic cell membrane. The initial OD increase was followed by a decrease when the majority of the cells had passed the blebbing stage. If we consider the similarities with the results presented here, especially the transient tendency of the μ_t increase, it is likely that membrane blebbing is responsible for the results of our study.

In flow cytometry apoptotic cells are also identified on the basis of changes in scattering. Whereas this study focused on backscattered light, cytometry registers forward and side (90° angle) scattering of single cells. In flow cytometry data analysis, the forward scatter signal is correlated with the cell size, and the side scatter signal is correlated with the cell's refractive and reflective properties and reveals optical inhomogeneity, such as that resulting from condensation of cytoplasm or nucleus and granularity. During the apoptotic process, there is a slight initial decrease in forward scatter (cell shrinkage and mitochondrial swelling), followed by an increase in side scatter (nuclear condensation and fragmentation). The formation of apoptotic bodies is characterized by a decrease in both forward and side scatter [45]. Accordingly, changes in light scatter properties can contribute to the rapid and easy identification of apoptotic cells in particular conditions.

Czarnota et al. used colchicine to image mitotic arrested cells, which would be normal cells with a condensed nucleus. Whereas the initial goal was to image cells with mere condensed nuclei, possibly also apoptosis was induced in the colchicine-treated cells. Unfortunately, under certain experimental conditions, colchicine is also described as an apoptosis inducer [46, 47].

Clinical implications and study limitations

The monitoring of apoptosis could play an important role in the clinic [1]. Apart from an apparent diagnostic value, online monitoring of apoptosis in response to treatment could greatly improve therapeutic efficacy in, e.g., skin cancer treatment.

Apoptosis also plays a role in cardiovascular disease. Apoptosis of vascular smooth muscle cells [48, 49] and macrophages [50] localizes in so-called vulnerable lesions, i.e. those lesions most likely to rupture, and at sites of actual ruptured plaques. In in vivo studies, induction of apoptosis in endothelial cells as well as in smooth muscle cells has been shown to result in thrombosis [51] and plaque rupture [52], respectively. However, before OCT can be used to detect vascular apoptosis, the specificity and sensitivity of the detection of cell death has to be investigated.

Although the loss of cell integrity during necrosis could be determined by flow cytometry, the identification of apoptosis in fibroblasts met with insurmountable difficulties. Flow cytometry was developed for the analysis of single cells that grow in suspension. Adherent cells, like the fibroblasts used in this study, are very difficult to analyse by cytometry due to clumping of the cells, and rupturing of cells when resuspending. Furthermore, it should be stressed that, because the cells become detached during late stages of apoptosis, many apoptotic cells may be selectively lost if the analysis is limited to the attached cells only [53].

Further research has to be done to elucidate the origin of light scattering by cells in order to address the question of the reason of rapid light scattering changes in dying cells, especially compared to the later observed apoptosis by biochemical methods. Chalut et al. showed that within 1.5 hours of apoptosis induction, the sub-cellular organization, described as the fractal dimension, rapidly decreases [54]. They also observed a biphasic response in time, which was possibly related to mitochondrial swelling, fission and fusion. Similarly, Mulvey et al. recently described rapid changes in scattering of suspensions of cells after induction of apoptosis [55]. Because the index of refraction of membranes is relatively high (~1.46) [56], changes in the membrane structure may have a relatively large effect on the scattering properties. Furthermore, the effect of dependent scattering, e.g. due to the packing of scatterers, may also influence the measurement of optical properties [57].

It remains to be defined whether the changes in light scatter properties are characteristic of apoptosis or whether they correspond to general features of cell death, whatever the mode of cell death considered. Conversely, OCT measurements as described in this study could be helpful in identifying the scatterers in cells, but other techniques based on elastic light scattering [58–60] or combined with Raman spectroscopy [61] may also be suitable.

Conclusion

The results from the cultured cells described in this study indicate the ability of OCT to detect and differentiate between viable, apoptotic and necrotic cells, based on their optical properties. This functional supplement to high-resolution OCT imaging can be of great clinical benefit, enabling the on-line monitoring of tissues or for feedback in cancer treatment. Furthermore, OCT imaging of apoptosis in the vascular wall might enhance the ability of OCT to detect the vulnerable plaque.

Acknowledgements This work was part of the research programme "Stichting voor Fundamenteel Onderzoek der Materie (FOM)', which is financially supported by the Nederlandse Organisatie voor Wetenschappelijk Onderzoek (NWO), and by the Netherlands Heart Foundation (grant 99.199). Dirk Faber and Maurice Aalders are supported by the Dutch Technology Foundation under grant AGT-7544 (NWO-Veni programme) and grant AGT-7547 (NWO-VIDI programme), respectively.

References

1. Vermes I, Haanen C (1994) Apoptosis and programmed cell death in health and disease. Adv Clin Chem 31:177–246
2. Kerr JF, Wyllie AH, Currie AR (1972) Apoptosis: a basic biological phenomenon with wide-ranging implications in tissue kinetics. Br J Cancer 26:239–257
3. Thompson CB (1995) Apoptosis in the pathogenesis and treatment of disease. Science 267:1456–1462
4. Vermes I, Haanen C, Reutelingsperger C (2000) Flow cytometry of apoptotic cell death. J Immunol Methods 243:167–190
5. Blankenberg FG, Katsikis PD, Tait JF, Davis RE, Naumovski L, Ohtsuki K, Kopiwoda S, Abrams MJ, Darkes M, Robbins RC, Maecker HT, Strauss HW (1998) In vivo detection and imaging of phosphatidylserine expression during programmed cell death. Proc Natl Acad Sci U S A 95:6349–6354
6. Zhao M, Beauregard DA, Loizou L, Davletov B, Brindle KM (2001) Non-invasive detection of apoptosis using magnetic resonance imaging and a targeted contrast agent. Nat Med 7:1241–1244

7. Czarnota GJ, Kolios MC, Abraham J, Portnoy M, Ottensmeyer FP, Hunt JW, Sherar MD (1999) Ultrasound imaging of apoptosis: high-resolution non-invasive monitoring of programmed cell death in vitro, in situ and in vivo. Br J Cancer 81:520–527
8. Huang D, Swanson EA, Lin CP, Schuman JS, Stinson WG, Chang W, et al (1991) Optical coherence tomography. Science 254:1178–1181
9. van der Meer FJ, Faber DJ, Perree J, Pasterkamp G, Baraznji Sassoon DM, van Leeuwen TG (2005) Quantitative optical coherence tomography of arterial wall components. Lasers Med Sci 20:45–51
10. Perlman H, Maillard L, Krasinski K, Walsh K (1997) Evidence for the rapid onset of apoptosis in medial smooth muscle cells after balloon injury. Circulation 95:981–987
11. Beuthan J, Minet O, Helfmann J, Herrig M, Muller G (1996) The spatial variation of the refractive index in biological cells. Phys Med Biol 41:369–382
12. Kravtsov VD, Fabian I (1996) Automated monitoring of apoptosis in suspension cell cultures. Lab Invest 74:557–570
13. Mourant JR, Canpolat M, Brocker C, Esponda-Ramos O, Johnson TM, Matanock A, Stetter K, Freyer JP (2000) Light scattering from cells: the contribution of the nucleus and the effects of proliferative status. J Biomed Opt 5:131–137
14. Shiffer Z, Zurgil N, Shafran Y, Deutsch M (2001) Analysis of laser scattering pattern as an early measure of apoptosis. Biochem Biophys Res Commun 289:1320–1327
15. Beauvoit B, Evans SM, Jenkins TW, Miller EE, Chance B (1995) Correlation between the light scattering and the mitochondrial content of normal tissues and transplantable rodent tumors. Anal Biochem 226:167–174
16. Prado A, Puyo C, Arlucea J, Goni FM, Arechaga J (1996) The turbidity of cell nuclei in suspension: a complex case of light scattering. J Colloid Interface Sci 177:9–13
17. Rollins AM, Kulkarni MD, Yazdanfar S, Ung-arunyawee R, Izatt JA (1998) In vivo video rate optical coherence tomography. Opt Express 3:219–229
18. van der Meer FJ, Faber DJ, Baraznji Sassoon DM, Aalders MC, Pasterkamp G, van Leeuwen TG (2005) Localized measurement of optical attenuation coefficients of atherosclerotic plaque constituents by quantitative optical coherence tomography. IEEE Trans Med Imaging 24:1369
19. Izatt JA, Hee MR, Owen GM, Swanson EA, Fujimoto JG (1994) Optical coherence microscopy in scattering media. Opt Lett 19:590–592
20. Faber DJ, van der Meer FJ, Aalders MCG, van Leeuwen TG (2004) Quantitative measurement of attenuation coefficients of weakly scattering media using optical coherence tomography. Opt Express 12:4353–4365
21. van Leeuwen TG, Faber DJ, Aalders MC, Aalders MC (2003) Measurement of the axial point spread function in scattering media using single-mode fiber-based optical coherence tomography. IEEE J Sel Top Quantum Electron 9:227–233
22. Abidor IG, Li LH, Hui SW (1994) Studies of cell pellets: I. Electrical properties and porosity. Biophys J 67:418–426
23. Watanabe T, Voyvodic JT, Chan-Ling T, Sagara H, Hirosawa K, Mio Y, Matsushima S, Uchimura H, Nakahara K, Raff MC (1997) Differentiation and morphogenesis in pellet cultures of developing rat retinal cells. J Comp Neurol 377:341–350
24. Yung LJ, Hall R, Pelinkovic D, Cassinelli E, Usas A, Gilbertson L, Huard J, Kang J (2001) New use of a three-dimensional pellet culture system for human intervertebral disc cells: initial characterization and potential use for tissue engineering. Spine 26:2316–2322
25. Grant S (1998) Ara-C: cellular and molecular pharmacology. Adv Cancer Res 72:197–233
26. Iacobini M, Menichelli A, Palumbo G, Multari G, Werner B, Del Principe D (2001) Involvement of oxygen radicals in cytarabine-induced apoptosis in human polymorphonuclear cells. Biochem Pharmacol 61:1033–1040
27. Kanno S, Higurashi A, Watanabe Y, Shouji A, Asou K, Ishikawa M (2004) Susceptibility to cytosine arabinoside (Ara-C)-induced cytotoxicity in human leukemia cell lines. Toxicol Lett 152:149–158
28. Dessi F, Pollard H, Moreau J, Ben Ari Y, Charriaut-Marlangue C (1995) Cytosine arabinoside induces apoptosis in cerebellar neurons in culture. J Neurochem 64:1980–1987
29. Manakova S, Puttonen KA, Raasmaja A, Mannisto PT (2003) Ara-C induces apoptosis in monkey fibroblast cells. Toxicol In Vitro 17:367–373
30. Vermes I, Haanen C, Steffens-Nakken H, Reutellingsperger C (1995) A novel assay for apoptosis flow cytometric detection of phosphatidylserine expression on early apoptotic cells using fluorescein labelled annexin V. J Immunol Methods 184:39–51
31. Bouffard DY, Momparler RL (1995) Comparison of the induction of apoptosis in human leukemic cell lines by 2′,2′-difluorodeoxycytidine (gemcitabine) and cytosine arabinoside. Leuk Res 19:849–856
32. Guchelaar HJ, Vermes I, Koopmans RP, Reutelingsperger CP, Haanen C (1998) Apoptosis- and necrosis-inducing potential of cladribine, cytarabine, cisplatin, and 5-fluorouracil in vitro: a quantitative pharmacodynamic model. Cancer Chemother Pharmacol 42:77–83
33. Stolzenberg I, Wulf S, Mannherz HG, Paddenberg R (2000) Different sublines of jurkat cells respond with varying susceptibility of internucleosomal DNA degradation to different mediators of apoptosis. Cell Tissue Res 301:273–282
34. Granville DJ, Hunt DWC (2000) Porphyrin-mediated photosensitization: taking apoptosis the fast lane. Curr Opin Drug Discov Devel 3:232–243
35. Barer R, Ross KFA (1953) Refractometry of living cells. Nature 171:720–724
36. Mourant JR, Freyer JP, Hielscher AH, Eick AA, Shen D, Johnson TM (1998) Mechanisms of light scattering from biological cells relevant to noninvasive optical-tissue diagnostics. Appl Opt 37:3586–3593
37. van de Hulst, H. C. (1981) Light scattering by small particles. Structure of matter series, Dover, New York
38. Valenzeno DP, Trank JW (1985) Measurement of cell lysis by light scattering. Photochem Photobiol 42:335–339
39. Wilson JD, Bigelow CE, Calkins DJ, Foster TH (2005) Light scattering from intact cells reports oxidative-stress-induced mitochondrial swelling. Biophys J 88:2929–2938
40. Wilson JD, Giesselman BR, Mitra S, Foster TH (2007) Lysosome-damage-induced scattering changes coincide with release of cytochrome C. Opt Lett 32:2517–1519
41. Narita M, Shimizu S, Ito T, Chittenden T, Lutz RJ, Matsuda H, Tsujimoto Y (1998) Bax interacts with the permeability transition pore to induce permeability transition and cytochrome c release in isolated mitochondria. Proc Natl Acad Sci U S A 95:14681–14686
42. Finucane DM, Bossy-Wetzel E, Waterhouse NJ, Cotter TG (1999) Bax-induced caspase activation and apoptosis via cytochrome c release from mitochondria is inhibitable by Bcl-xL. J Biol Chem 274:2225–2233
43. Kroemer G, Galluzzi L, Brenner C (2007) Mitochondrial membrane permeabilization in cell death. Physiol Rev 87:99–163
44. Boustany NN, Tsai Y-C, Pfister B, Joiner WM, Oyler GA, Thakor NV (2004) BCL-xL-dependent light scattering by apoptotic cells. Biophys J 87:4163–4171
45. Darzynkiewicz Z, Bedner E, Smolewski P (2001) Flow cytometry in analysis of cell cycle and apoptosis. Semin Hematol 38:179–193
46. Bonfoco E, Ceccatelli S, Manzo L, Nicotera P (1995) Colchicine induces apoptosis in cerebellar granule cells. Exp Cell Res 218:189–200

47. Cervinka M, Cerman J, Rudolf E (2004) Apoptosis in Hep2 cells treated with etoposide and colchicine. Cancer Detect Prev 28:214–226
48. Bauriedel G, Hutter R, Welsch U, Bach R, Sievert H, Luderitz B (1999) Role of smooth muscle cell death in advanced coronary primary lesions: implications for plaque instability. Cardiovasc Res 41:480–488
49. Dhume AS, Soundararajan K, Hunter WJ III, Agrawal DK (2003) Comparison of vascular smooth muscle cell apoptosis and fibrous cap morphology in symptomatic and asymptomatic carotid artery disease. Ann Vasc Surg 17:1–8
50. Kolodgie FD, Narula J, Burke AP, Haider N, Farb A, Hui-Liang Y, Smialek J, Virmani R (2000) Localization of apoptotic macrophages at the site of plaque rupture in sudden coronary death. Am J Pathol 157:1259–1268
51. Durand E, Scoazec A, Lafont A, Boddaert J, Al Hajzen A, Addad F, et al (2004) In vivo induction of endothelial apoptosis leads to vessel thrombosis and endothelial denudation: a clue to the understanding of the mechanisms of thrombotic plaque erosion. Circulation 109:2503–2506
52. von der Thusen JH, van Vlijmen BJ, Hoeben RC, Kockx MM, Havekes LM, van Berkel TJ, et al. (2002) Induction of atherosclerotic plaque rupture in apolipoprotein E-/- mice after adenovirus-mediated transfer of P53. Circulation 105:2064–2070
53. Bedner E, Li X, Gorczyca W, Melamed MR, Darzynkiewicz Z (1999) Analysis of apoptosis by laser scanning cytometry. Cytometry 35:181–195
54. Chalut KJ, Ostrander JH, Giacomelli MG, Wax A (2009) Light scattering measurements of subcellular structure provide non-invasive early detection of chemotherapy-induced apoptosis. Cancer Res 69:1199–1204
55. Mulvey CS, Curtis AL, Singh SK, Bigio IJ (2007) Elastic scattering spectroscopy as a diagnostic tool for apoptosis in cell cultures. IEEE J Sel Top Quantum Electron 13:1663–1670
56. van Manen HJ, Verkuijlen P, Wittendorp P, Subramaniam V, van den Berg TK, Roos D, et al (2008) Refractive index sensing of green fluorescent proteins in living cells using fluorescence lifetime imaging microscopy. Biophys J 94:L67–L69
57. Faber DJ, van Leeuwen TG (2009) Are quantitative attenuation measurements of blood by optical coherence tomography feasible? Opt Lett 34:1435–1437
58. Amelink A, Sterenborg HJCM (2004) Measurement of the local optical properties of turbid media by differential path-length spectroscopy. Appl Opt 43:3048–3054
59. Amelink A, Sterenborg HJCM, Bard MPL, Burgers SA (2004) In vivo measurement of the local optical properties of tissue by use of differential path-length spectroscopy. Opt Lett 29:1087–1089
60. Reif R, A'Amar O, Bigio IJ (2007) Analytical model of light reflectance for extraction of the optical properties in small volumes of turbid media. Appl Opt 46:7317–7328
61. Patil CA, Bosschaart N, Keller MD, van Leeuwen TG, Mahadevan-Jansen A (2008) Combined Raman spectroscopy and optical coherence tomography device for tissue characterization. Opt Lett 33:1135–1137